Sputtered Porous Li-Fe-P-O Film Cathodes Prepared by Radio Frequency Sputtering for Li-ion Microbatteries

V. Sugiawati, Florence Vacandio, C. Perrin-Pellegrino, A. Galeyeva, A. Kurbatov, T. Djenizian

SCIENTIFIC REPORTS
nature research

OPEN

Sputtered Porous Li-Fe-P-O Film Cathodes Prepared by Radio Frequency Sputtering for Li-ion Microbatteries

Received: 16 May 2019
Accepted: 9 July 2019
Published online: 01 August 2019

V. A. Sugiawati[1], F. Vacandio[2], C. Perrin-Pellegrino[3], A. Galeyeva[4], A. P. Kurbatov[4] & T. Djenizian[1]

The increasing demands from micro-power applications call for the development of the electrode materials for Li-ion microbatteries using thin-film technology. Porous Olivine-type $LiFePO_4$ (LFP) and NASICON-type $Li_3Fe_2(PO_4)_3$ have been successfully fabricated by radio frequency (RF) sputtering and post-annealing treatments of LFP thin films. The microstructures of the LFP films were characterized by X-ray diffraction and scanning electron microscopy. The electrochemical performances of the LFP films were evaluated by cyclic voltammetry and galvanostatic charge-discharge measurements. The deposited and annealed thin film electrodes were tested as cathodes for Li-ion microbatteries. It was found that the electrochemical performance of the deposited films depends strongly on the annealing temperature. The films annealed at 500 °C showed an operating voltage of the porous LFP film about 3.45 V vs. Li/Li^+ with an areal capacity of 17.9 µAh cm^{-2} µm^{-1} at C/5 rate after 100 cycles. Porous NASICON-type $Li_3Fe_2(PO_4)_3$ obtained after annealing at 700 °C delivers the most stable capacity of 22.1 µAh cm^{-2} µm^{-1} over 100 cycles at C/5 rate, with an operating voltage of 2.8 V vs. Li/Li^+. The post-annealing treatment of sputtered LFP at 700 °C showed a drastic increase in the electrochemical reactivity of the thin film cathodes vs. Li^+, leading to areal capacity ~9 times higher than as-deposited film (~27 vs. ~3 µAh cm^{-2} µm^{-1}) at C/10 rate.

Li-ion microbatteries have emerged a new direction for powering the miniaturized modern devices, for instance RFID tags, implantable medical devices, microsensors, and smart cards. In order to advance towards the fabrication of all-solid-state thin film microbatteries, numerous studies have been reported to find innovative cathode and anode materials. Most of reports have been largely devoted to anode materials such as self-organized TiO_2 nanotubes[1,2], silicon nanowires[3], Cu_2Sb[4], aluminum nanorods[5], carbon nanotubes[6,7], and $LiNiVO_4$[8]. Besides the anode materials, exploiting the cathode materials are very crucial to realize the fabrication of full cell Li-ion microbatteries. Iron-based phosphate especially olivine-type $LiFePO_4$ (LFP) becomes a popular cathode as it is known to be cheap, abundant, low toxic, and thermally stable[9]. The strong Fe-O covalent bonds in LFP cathodes has such a special characteristic compared to layered $LiCoO_2$-type materials[10]. Indeed, this covalent bond greatly improve the stability of O in the lattice, thus increasing the reliability of the materials.

In the field of thin-film microbatteries, study the properties of the pure active layers deposited onto the current collectors is essential since neither binder nor conductive additive are utilized[11–13]. By using the thin film cathodes, the intrinsic drawbacks such as a low electronic conductivity and low Li^+ diffusion mobility can also be suppressed because the thickness of the cathode material is considerably reduced[14–16]. Much studies have reported the growth of thin-film electrodes by various techniques such as pulsed laser deposition (PLD)[17–22], sputtering[23,24] and sol-gel[25–27]. Among these different approaches, radio frequency (RF) sputtering technique is considered to

[1]Mines Saint-Etienne, Center of Microelectronics in Provence, Department of Flexible Electronics, F – 13541, Gardanne, France. [2]Aix-Marseille Université, CNRS, Electrochemistry of Materials Research Group, MADIREL, UMR 7246, F-13397, Marseille, Cedex 20, France. [3]Aix-Marseille Université, Institut Matériaux Microélectronique Nanoscience de Provence (IM2NP), Faculté des Sciences, Campus de Saint-Jérôme, Avenue Escadrille Normandie Niemen - Case 142, F-13397, Marseille, Cedex, France. [4]Al-Farabi Kazakh National University, Center of Physical-Chemical Methods of Research and Analysis, Tole bi str., 96A, Almaty, Kazakhstan. Correspondence and requests for materials should be addressed to T.D. (email: thierry.djenizian@emse.fr)

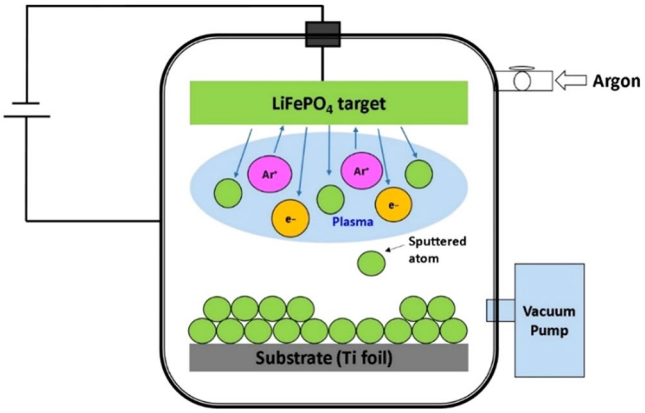

Figure 1. Schematic representation of a RF sputtering system.

be the most versatile way to fabricate thin-film cathodes[16,28] because the sputtering parameters are easily controlled to obtain a good quality film, such as sputtering power, argon pressure, and substrate temperature during deposition.

More recently, RF sputtering have attracted substantial attention in the fabrication of the flexible and transparent thin-film batteries. For example, Lee *et al.*[29] reported a flexible battery applied on contact lens using LFP cathode material deposited on the flexible polyimide substrate by RF sputtering, the thin film reached 63.8% of the theoretical capacity without carbon coating and the cell showed stable performance under wet conditions. Also, Oukassi *et al.*[30] deposited transparent thin film batteries layers using RF sputtering, a discharge capacity of 0.15 mAh at C/2 rate with an average capacity loss of solely 0.15% per cycle can be obtained.

Due to a strong research interest focused on searching for lithium transition metal phosphates as cathode materials, NASICON type-$Li_3Fe_2(PO_4)_3$ has been reported of having a high lithium mobility and can intercalate up to two moles of lithium within the structure[31]. Besides a theoretical capacity of 128 mAh g^{-1} [32], $Li_3Fe_2(PO_4)_3$ cathode is currently attracting considerable interest due to several advantages such as low toxicity, low cost, good ionic conductivity, and large natural abundance[33]. Furthermore, the structure of the NASICON type-$Li_3Fe_2(PO_4)_3$ is more stable than that of olivine-type $LiFePO_4$[34] and its synthesis is easier as it can be prepared directly in air. NASICON type-$Li_3Fe_2(PO_4)_3$ have been commonly synthesized via various methods such as solid-state reactions[35], hydrothermal[36], sol-gel combustion[32] and ultrasonic spray pyrolysis[37]. However, there are only limited reports regarding the $Li_3Fe_2(PO_4)_3$ film deposited by RF Sputtering[12]. In the present work, we propose to study the effect of annealing temperature on RF sputtered LFP thin-films in terms of morphology, composition, structure, and electrochemical properties. We show that the thermal treatment performed at 700 °C in air leads to the formation of porous $Li_3Fe_2(PO_4)_3$ showing the best electrochemical performance and therefore being a good candidate as a cathode for Li-ion microbatteries.

Results and Discussion

Structural and chemical characterization. The schematic representation of the sputtering system is illustrated in Fig. 1. The sputtering process can be briefly described as follows: an inert argon gas is introduced in the vacuum chamber and the ionization process leads to the formation of a plasma. Then, the energized ions hitting the LFP target (cathode) eject out adatoms that are deposited on the substrate to form a thin film. Various parameters such as the nature of the substrate, the sputtering power, the argon pressure, the duration, and the deposition temperature have significant influences on the growth rate and features of the deposited film[14].

In this work, a sputtering power of 3 W cm^{-2} and argon pressure of 7 mTorr during 12 hours of deposition was employed to obtain smooth and dense layers as well as a better adhesion between the films and the substrates. Owing to a low deposition rate, 12 hours of deposition is required to obtain LFP films with a sufficient thickness for the targeted application. The XRD pattern of the commercial LFP target and as-deposited film are plotted in Fig. 2a. Obviously, the initial target has well-defined peaks corresponding to the Olivine $LiFePO_4$ (JCPDS File No. 040-1499). However, after deposition at room temperature, only Ti peaks can be identified suggesting that the material is amorphous. The amorphous nature of the thin films deposited without heating treatment, either substrate heating during deposition or post-annealing have been reported in previous studies[12,14]. Thus, the thermal treatment step is essential because the crystalline materials are known for their better electrochemical reactivities versus Li ions[38].

Figure 2b,c display the SEM images of the thin films deposited at 3 W cm^{-2} W during 12 hours. As-deposited film shows a dense layer with a thickness of approximately 1.6 µm that corresponds to a growth rate of 2.2 nm min^{-1}. EDX analysis after deposition (Fig. 2d) revealed a Fe:P atomic ratio of 14.33(1): 14.58(1), which is in agreement with the LFP formula. To further study in detail the effects of the annealing temperature, the as-deposited LFP films were annealed at 400 °C, 500 °C, 600 °C, and 700 °C, respectively in air atmosphere for one hour. In agreement with the previous studies, as-deposited films show poor crystallinity. As the films are annealed, the adsorbed atom on the surface of the films are activated and rearranged to form ordered crystal structure[39]. The XRD patterns for the LFP films are gathered in Fig. 3 for analyzing the effects of the thermal treatment at various temperatures on their crystal structure. At first glance, the typical peaks ascribable to crystalline

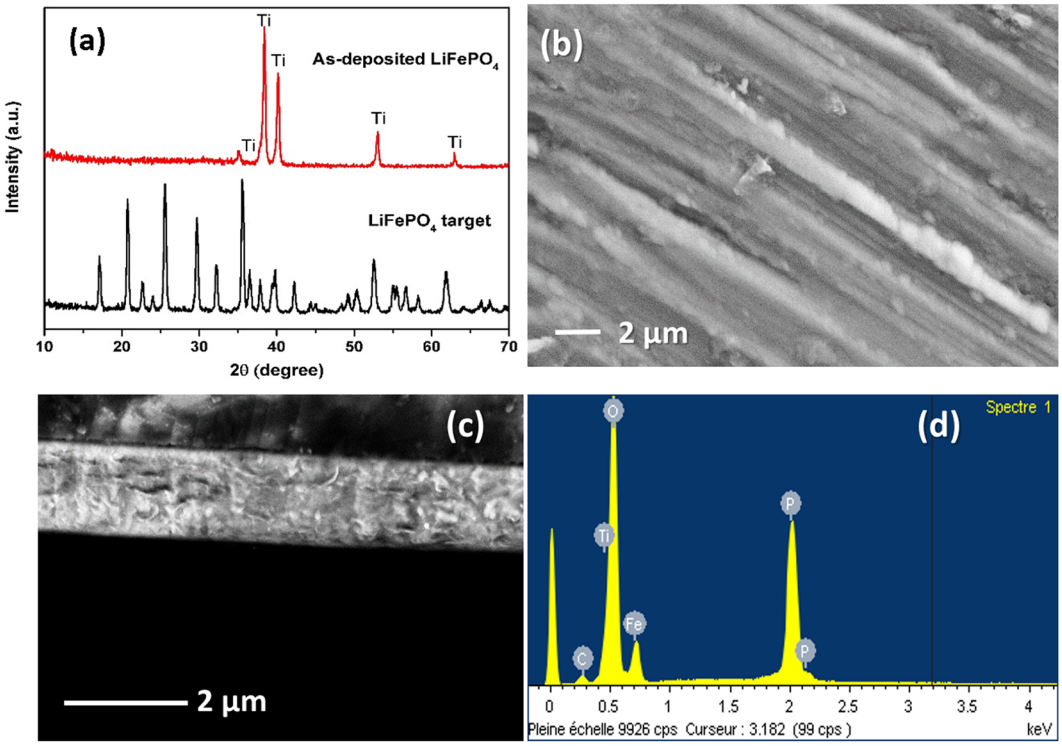

Figure 2. XRD patterns of the commercial LFP target and as-deposited LFP film (**a**), SEM images of as-deposited LFP film from the top view (**b**), and cross-sectional view (**c**) and EDX analysis of the as-deposited LFP film (**d**).

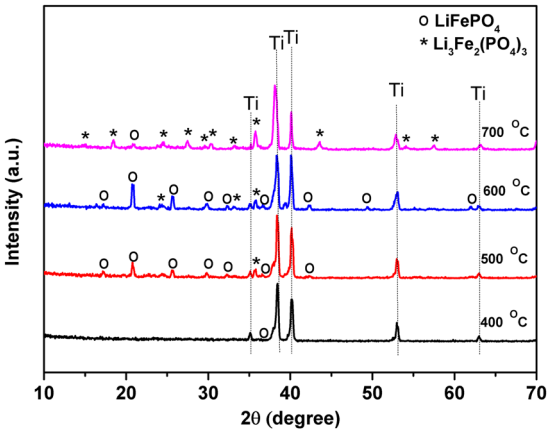

Figure 3. XRD patterns of LFP thin films annealed at various temperatures in air for one hour.

LFP and $Li_3Fe_2(PO_4)_3$ phases can be detected at elevated temperatures. The amorphous nature of LFP is evidenced for the film annealed at 400 °C since only Ti peaks are visible. This result confirms that annealing temperature higher than 400 °C is required to crystallize LFP thin film[13]. As the temperature was increased to 500 °C, several characteristic peaks of 2θ suited at 17.21°, 20.82°, 25.65°, 29.87° and 32.36° marked as symbol (o) are attributed to the (0 2 0), (0 1 1), (0 2 1), (1 2 1) and (0 3 1) planes of LFP phase. Besides the presence of LFP peaks, two small $Li_3Fe_2(PO_4)_3$ peaks with low intensities marked as symbol (*) are also detected at 2θ of 24.4° and 35.8° suggesting that the decomposition of $LiFePO_4$ phase has also started. Nevertheless, crystalline LFP seems to be the most predominant phase at 500 °C. This is probably due to a slow heating rate that is applied during annealing treatment. As reported elsewhere[40], the heating rate plays an important role in decelerating a second phase formation. It is important to note that in our work the films were heated at 2 °C min^{-1} to avoid the fast formation of $Li_3Fe_2(PO_4)_3$ phase due to the LFP sensibility to air atmosphere. Thus, the LFP phase can be clearly detected at 500 °C after annealing in air atmosphere. Presumably, $Li_3Fe_2(PO_4)_3$ phase might be quickly obtained when the heating rate is faster than 2 °C min^{-1} in air. When the annealing temperature further raised to 600 °C, more $Li_3Fe_2(PO_4)_3$ (JCPDS

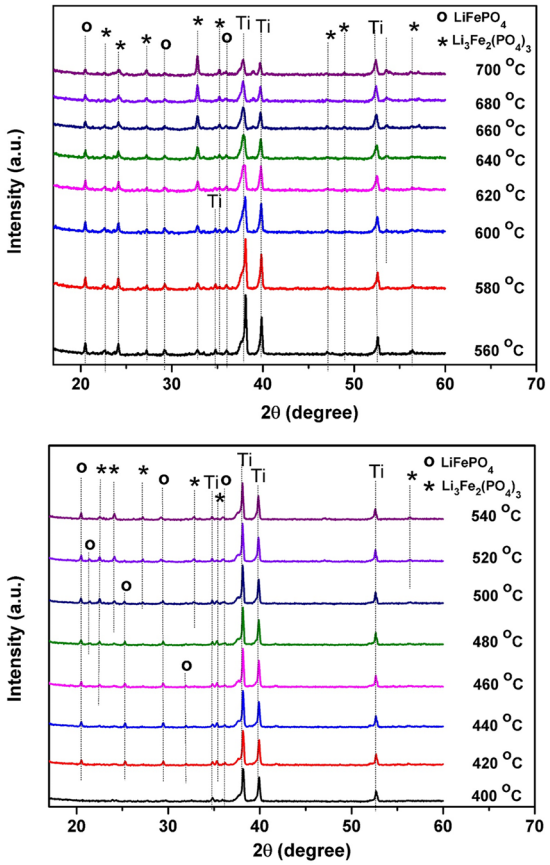

Figure 4. *In-situ* XRD patterns ($\lambda = 1.54$ Å) of as-deposited LFP film during thermal annealing performed between 400 and 700 °C by step of 20 °C.

file no. 047-0107) peaks have appeared. The annealed films at 600 °C are assumed to be composed of mixed LFP and $Li_3Fe_2(PO_4)_3$ phases. In a good agreement with the previous reports[17,18,24,40], the optimum annealing temperature for the crystallization of LFP was 500 °C. As expected, by increasing the annealing temperature up to 700 °C, almost all phases are transformed to $Li_3Fe_2(PO_4)_3$ due to the oxidation of Fe^{2+} by oxygen from air according to Eq. (1) [12].

$$12LiFePO_4 + 3O_2 \rightarrow 4Li_3Fe_2(PO_4)_3 + 2Fe_2O_3 \quad (1)$$

Another LFP phase with very low intensity at $2\theta = 20.82°$ is detected as minor phase. However, the peak intensity appears to be weakening at this temperature. As previously reported[41], encouraging results on the electrochemically active $Li_3Fe_2(PO_4)_3$ phase that obtained after annealing at 700 °C have been studied in the form of composite electrodes carrying polymer binder and carbon additive. NASICON-type $Li_3Fe_2(PO_4)_3$ can be considered as an interesting cathode material for Li-ion batteries by hosting about 2 additional Li^+ (Fe^{3+}/Fe^{2+} redox couple) with great reversibility at a voltage plateau of around 2.8 V[23–27]. However most reports on this material focus on composite $Li_3Fe_2(PO_4)_3$ cathodes prepared by slurry coatings instead of thin films.

In-depth structural studies have been also carried out by *in-situ* XRD experiments. The purpose of this particular structural analysis is to follow the evolution of the formed phases at elevated temperature after deposition time of 3 hours. The different XRD patterns given in Fig. 4 were acquired during annealing process between 400 °C and 700 °C using steps of 20 °C. Starting from 400 °C, a low intensity peak corresponding to LFP appeared at $2\theta = 35.90°$. In fact, $Li_3Fe_2(PO_4)_3$ starts to crystallize at 420 °C which is shown by the presence of a small peak at $2\theta = 35.36°$ with a low crystallinity. Both $Li_3Fe_2(PO_4)_3$ and LFP peaks can be clearly observed in the temperature range between 560 °C and 640 °C, mainly the stronger peak intensity located at $2\theta = 20.82°$ for LFP phase and $2\theta = 24.14°$ for $Li_3Fe_2(PO_4)_3$ phase. Then, the intensities of both peaks are getting weaker and even disappeared when annealing temperatures are higher than 640 °C or lower than 560 °C. This temperature range is considered to be less preferred for the Li ion intercalation/de-intercalation in the cathode materials. At the temperature below 560 °C, the presence of LFP phase is more pronounced, on the contrary when the annealing temperature is higher than 640 °C the appearance of $Li_3Fe_2(PO_4)_3$ phase becomes predominant. Similar results on the LFP powders were observed by Hamelet *et al.*[41] and Delacourt *et al.*[42], demonstrating the significant decomposition of the LFP phase occurred on thermal treatment at temperatures greater than ~ 500 °C and the progressive sharpening peaks for the $Li_3Fe_2(PO_4)_3$ can be observed afterwards. Bünting *et al.*[43] reported that the Ti interdiffusion occured during the crystallization process of the LFP thin film, leading to the $LiTi_2(PO_4)_3$ (LTP) phase formation. From the XRD

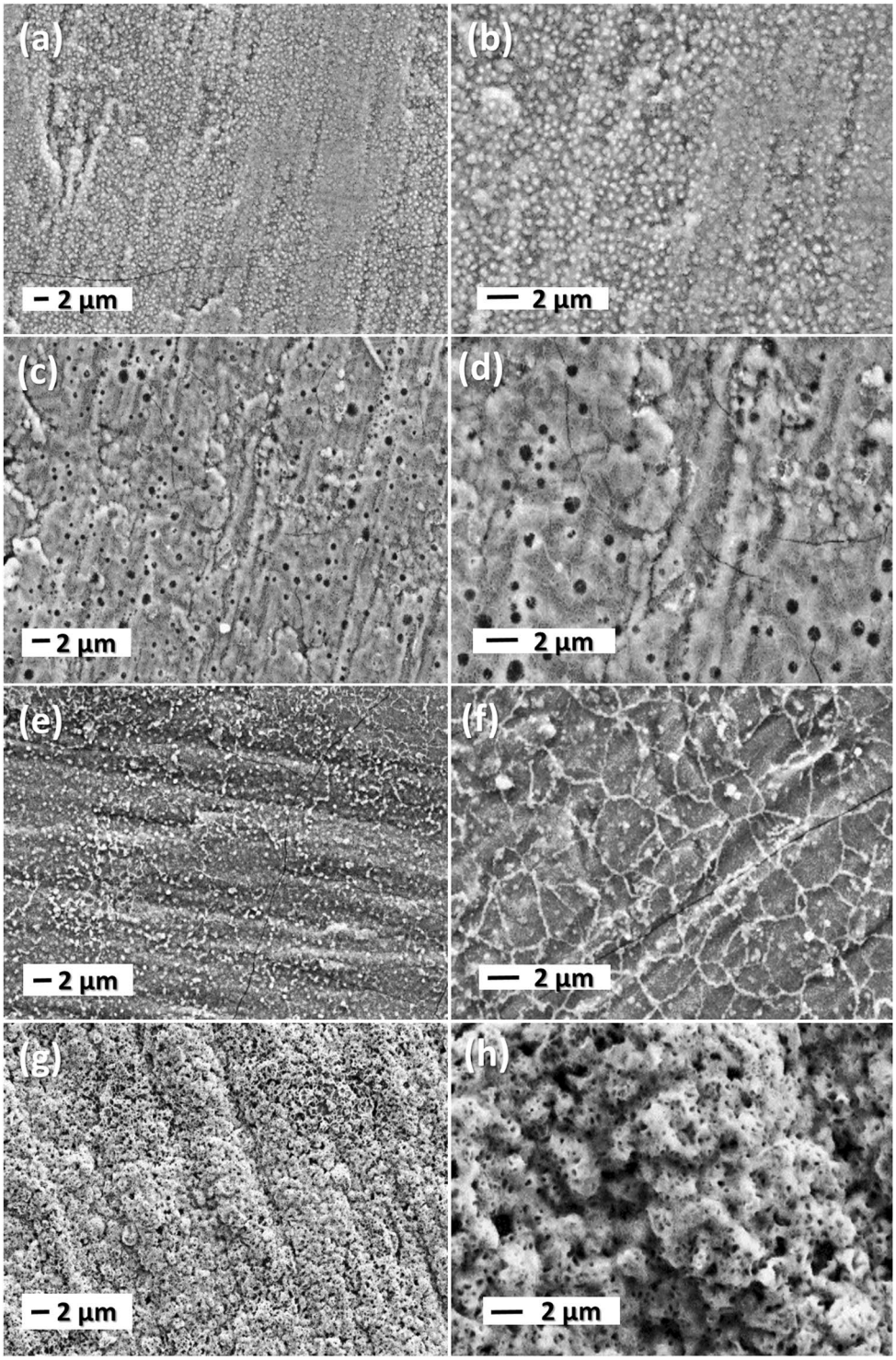

Figure 5. SEM images the annealed films at different temperatures LFP-400 (**a**,**b**), LFP-500 (**c**,**d**), LFP-600 (**e**,**f**) and LFP-700 (**g**,**h**).

pattern, the reflection peaks at $2\theta = 20.82°$ and $2\theta = 24.4°$ which overlap with the reflection peaks of LFP and $Li_3Fe_2(PO_4)_3$ are characteristics for LTP phase[44].

As the electrochemical performance of electrodes are often driven by their morphology, the examination of thin-films was performed by SEM. Figure 5 shows the surface of the annealed thin films. Apparently, the roughness increases with increasing of the annealing temperature.

According to the SEM examinations, LFP-400 is composed of small grains and exhibits a rough surface due to an inhomogeneous size distribution of particles (Fig. 5a,b). As the temperature is raised to 500 °C, the surface is characterized by the presence of large pores with various diameters (Fig. 5c,d), suggesting the formation

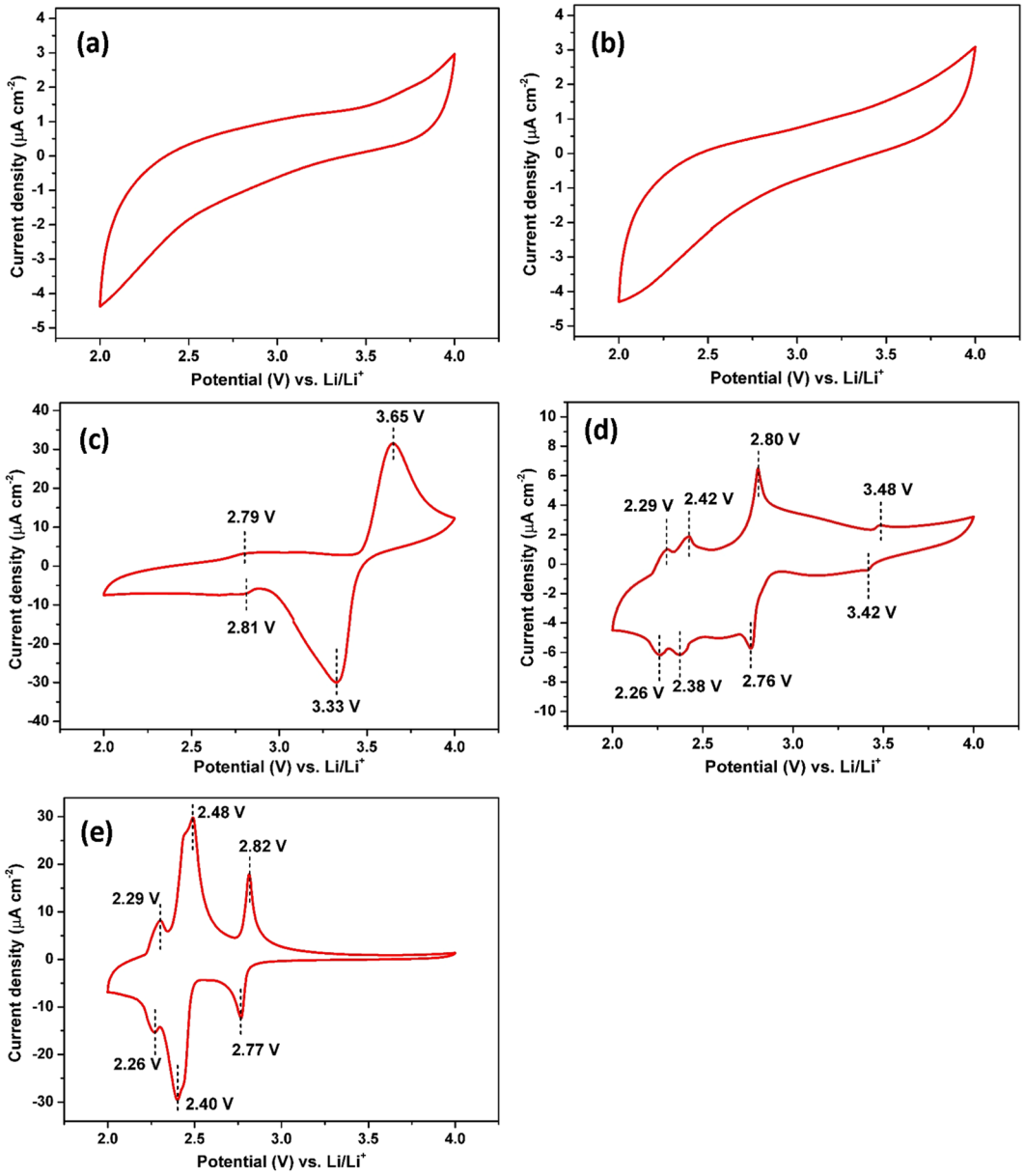

Figure 6. Cyclic voltammograms (1st cycle) of the LFP-0 film (**a**), LFP-400 (**b**), LFP-500 (**c**), LFP-600 (**d**) and LFP-700 (**e**).

of crystalline LFP phase[40,45]. As the temperature reaches 600 °C, the microstructured deposit is highlighted by appearance of grain boundaries with various grain sizes. After annealing at 700 °C, the surface becomes coarse and highly porous, which is consistent with the formation of the NASICON-type $Li_3Fe_2(PO_4)_3$ phase[12]. From the above results, it is interesting to note that the texture of LFP thin films shows some cracks except for the sample annealed at the highest temperature.

Electrochemical characterization. Cyclic voltammetry (CV) experiments were performed to evaluate the influence of the annealing process on the reactivity of LFP films with Li^+. Figure 6 shows the voltammograms obtained from the first cycle. No redox peak can be identified for LFP-0 (Fig. 6a) confirming that amorphous LFP is not electrochemically active. A similar behavior is observed for LFP-400 (Fig. 6b) suggesting that amorphous LFP is predominant despite the detection of a small peak by *in-situ* XRD which is attributed to the crystalline LFP phase. The LFP-500 film showed a well-defined peak pair and reversible redox peaks at 3.65 V and 3.33 V vs. Li/Li^+ corresponding to the anodic and cathodic peaks, respectively (Fig. 6c). These peaks are typical for the oxidation and reduction reactions of olivine-type $LiFePO_4$ material with Li^+ according to Eqs (2) and (3)[46].

$$\text{Oxidation: } LiFePO_4 - xLi^+ - xe^- \rightarrow xFePO_4 + (1 - x)LiFePO_4 \quad (2)$$

$$\text{Reduction: } FePO_4 + xLi^+ + xe^- \rightarrow xLiFePO_4 + (1 - x)LiFePO_4 \quad (3)$$

The low potential difference between the oxidation and reduction peaks (ΔEp) about 0.32 V vs. Li/Li^+ indicates that the film reveals a good electrochemical reversibility for Li^+ intercalation/de-intercalation. In addition, a broad peak pair with very low absolute current densities can also be observed at 2.79 V for the oxidation peak and 2.81 V for the reduction peak. These peaks correspond to the reaction of Li ions with the $Li_3Fe_2(PO_4)_3$ phase.

As the annealing temperature increases from 500 °C to 600 °C, a small oxidation peak at 3.48 V and a reduction peak at 3.42 V which are attributed to the two-phase transformation of the (Fe^{3+}/Fe^{2+}) redox couple due to the reversible intercalation of Li ions in the LFP crystal structure (Fig. 6d) are progressively vanished. This result is in good agreement with the XRD data showing that the LFP phase is clearly observable at 600 °C while the complete transformation into $Li_3Fe_2(PO_4)_3$ phase has yet to be occurred. In addition, a pair of anodic and cathodic peaks at around 2.29 V and 2.26 V vs. Li/Li^+ could be attributed to the formation of the iron tavorite phase $LiFePO_4(OH)$[12,47–49] according to Eq. (4)

$$2LiFePO_4 + 2H_2O \rightarrow 2LiFePO_4(OH) + H_2 \quad (4)$$

Thin film annealed at 700 °C (Fig. 6e) reveals a peak pair, a reduction peak at 2.77 V and an oxidation peak at 2.82 V which are attributed to the reversible intercalation reactions of Li^+ ions into $Li_3Fe_2(PO_4)_3$ as described by Eq. (5)[12].

$$Li_4Fe_2(PO_4)_3 = Li^+ + Li_3Fe_2(PO_4)_3 + e- \quad (5)$$

The cathodic and anodic peaks are symmetric and have similar current density values, indicating the excellent degree of reversibility. In a good agreement with the XRD analysis, due to the interdiffusion between the Ti and the deposited LFP thin film, the additional cathodic peak at 2.38 V and anodic peak at 2.42 V are observable at 600 °C and 700 °C which are characteristics for the $LiTi_2(PO_4)_3$[44] phase, according to Eq. (6)

$$Li_3Ti_2(PO_4)_3 = LiTi_2(PO_4)_3 + 2Li^+ + 2e^- \quad (6)$$

Preliminary CV results highlight that LFP thin films performances are strongly related to their structure and morphology. Indeed, the capacities of thin films prepared under different conditions varied significantly. Figure 7 shows the typical charge-discharge profiles of the five cathode thin films in the potential range 2–4 V at a current rate of C/10. In accordance with the CV curves, no voltage plateau can be observed for LFP-0 and LFP-400, delivering very low capacity values (<10 μAh cm^{-2} μm^{-1}). More remarkably, a couple of defined charge-discharge plateaus at 3.3 and 3.5 V are clearly seen at 500 °C corresponding to the reversible intercalation of lithium ions in crystallized $LiFePO_4$. These charge-discharge plateaus are fully consistent with the peaks of the CV curves. In many previous reports, crystalline LFP films can be obtained after annealing under inert atmosphere. In this work, the presence of the LFP phases can be detected after annealing treatment in air atmosphere. This result suggests that the phase transformation is slower, probably due to the low heating rate applied during the annealing treatment as previously mentioned. The capacities values for the 1st, 2nd, and 3rd cycles are 39 μAh cm^{-2} μm^{-1}, 37 μAh cm^{-2} μm^{-1} and 37 μAh cm^{-2} μm^{-1} with the corresponding coulombic efficiencies of 88%, 90% and 88%, respectively. The slight decrease of the coulombic efficiency is probably due to the small amount of $Li_3Fe_2(PO_4)_3$ phase that has been evidenced by XRD analysis.

For LFP-600, the voltage plateau around 2.8 V is ascribed to the reaction implying the $Li_3Fe_2(PO_4)_3$ phase. The presence of a short plateau at 3.5 V can be attributed to the low amount of crystalline LFP. The capacities of the LFP film annealed at 600 °C for the 1st, 2nd, and 3rd cycles are 27 μAh cm^{-2} μm^{-1}, 20 μAh cm^{-2} μm^{-1} and 18 μAh cm^{-2} μm^{-1} and the coulombic efficiencies are 57%, 80% and 84%, respectively. The low coulombic efficiency obtained in the 1st cycle could be explained by the mixed phases. In addition, the LFP film annealed at 700 °C revealed a well-defined plateau around 2.4 V which indicates the Li ions insertion into the $LiTi_2(PO_4)_3$ lattice structure and another plateau appeared at 2.8 Vcorresponds to redox reactions involving the $Li_3Fe_2(PO_4)_3$ phase[50–52]. The capacities of the film for the 1st, 2nd, and 3rd cycles are 31 μAh cm^{-2} μm^{-1}, 28 μAh cm^{-2} μm^{-1} and 27 μAh cm^{-2} μm^{-1}, while the associated coulombic efficiencies can reach 83%, 90% and 92%, respectively. Beyond the influence of the chemical and structural composition, the enhanced electrochemical properties of LFP-500 and LFP-700 can be explained by the porosity of the both layers. Actually, it has been reported that the use of porous electrodes can improve the electrochemical performance of batteries owing to the larger electrode/electrolyte interface[53,54]. In the present case, the porous nature of the LFP-500 and LFP-700 films is supposed to promote the penetration of the electrolyte providing more reaction electrochemical actives sites for the lithium ions intercalation/de-intercalation owing to larger accessible surface of the thin films. This is beneficial to improve the Li ion exchange between the LFP film electrode and electrolyte because the pores serve as channels for fast lithium supply[55].

In order to have a better insight into the potential use of annealed LFP layer as cathode materials, rate capability and long-term cycling tests were carried out. Figure 8a confirms that LFP-400 film provides the lowest capacity values attaining only 2 μAh cm^{-2} μm^{-1} at the 50th cycle. LFP-500 film exhibits the highest discharge capacities up to the 90th cycle but this cathode is subjected to a continuous capacity loss with a drop after the 80th cycle. The capacities obtained at the 1st, 2nd, and 100th cycle are 36 μAh cm^{-2} μm^{-1}, 35 μAh cm^{-2} μm^{-1}, and 18 μAh cm^{-2} μm^{-1}, respectively. Thus, only half of the initial capacity is retained after 100 cycles. It can be noticed that similar behavior regarding the capacity fading has been reported for the annealed $LiNi_{1/3}Co_{1/3}Mn_{1/3}O_2$ thin films at 500 °C[22]. Such a low cycling stability may be ascribed to the poor adhesion strength between the thin film and the substrate that are combined to the presence of cracks, leading to the detachment of the layer from the

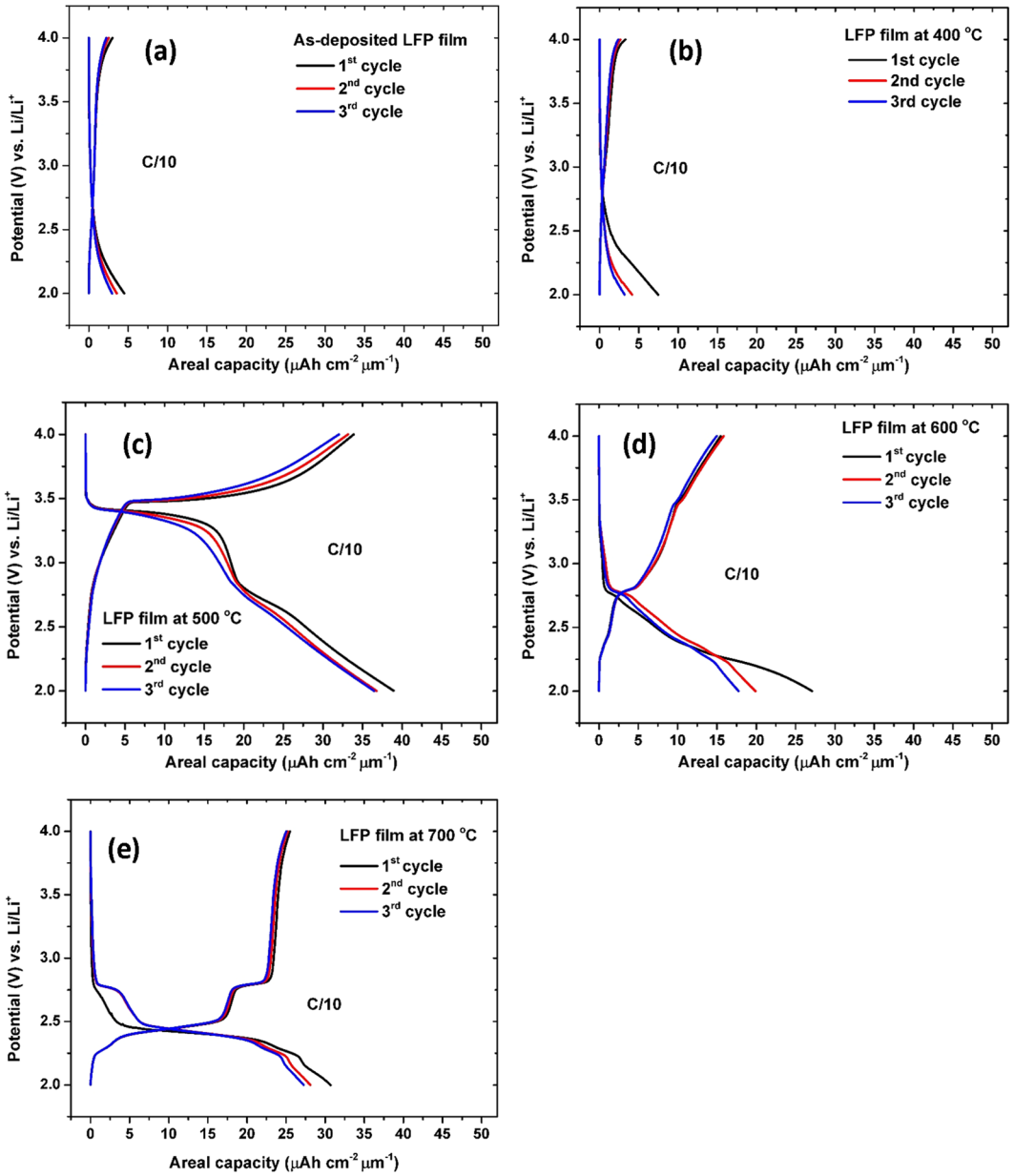

Figure 7. Charge-discharge profiles of the LFP-0 film (**a**), LFP-400 film (**b**), LFP-500 film (**c**), LFP-600 film (**d**) and LFP-700 film (**e**).

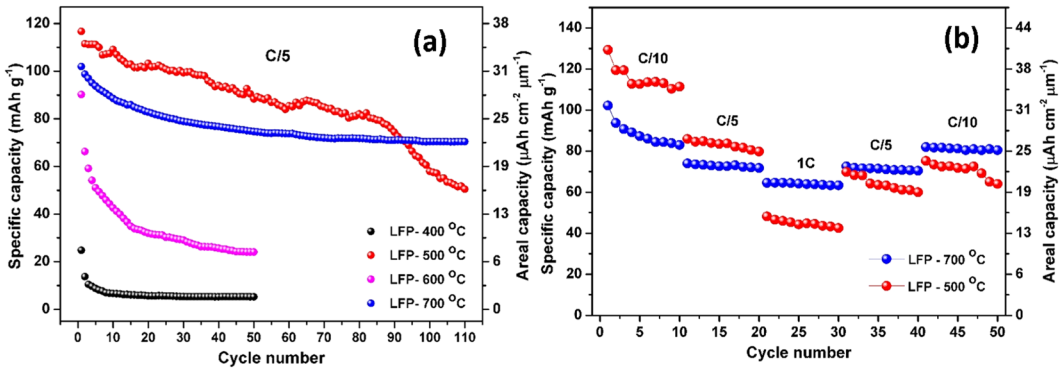

Figure 8. Long-term cycling stability study showing capacity versus the cycle number at C/5 rate for the various annealed LFP thin films (**a**), and rate capability of LFP-500 and LFP-700 films at multiple C-rates (**b**).

	400 °C	500 °C	600 °C	700 °C
Discharge capacity of the 1st cycle ($\mu Ah\ cm^{-2}\ \mu m^{-1}$)	8	36	29	32
Discharge capacity of the 50th cycle ($\mu Ah\ cm^{-2}\ \mu m^{-1}$)	2	28	8	24
Discharge capacity of the 100th cycle ($\mu Ah\ cm^{-2}\ \mu m^{-1}$)	—	18	—	22
Capacity retention (%) 1st–50th cycle	25	78	29	75
Capacity retention (%) 1st–100th cycle	—	50	—	70

Table 1. Electrochemical properties of LFP films annealed at various temperatures.

current collector and the subsequent loss of electrical contact. For the LFP-600 film, the first discharge capacity is relatively high (29 $\mu Ah\ cm^{-2}\ \mu m^{-1}$) but severely drops to reach only 8 $\mu Ah\ cm^{-2}\ \mu m^{-1}$ after the 50th cycle. This behavior could be attributed to the presence of cracks and mixed unstable $LiFePO_4$ and $Li_3Fe_2(PO_4)_3$ phases. Finally, LFP-700 film shows the best cycling stability. The capacities obtained for the LFP-700 were found to be 32 $\mu Ah\ cm^{-2}\ \mu m^{-1}$ for the first cycle and 22 $\mu Ah\ cm^{-2}\ \mu m^{-1}$ for the 100th cycle corresponding to a capacity retention of around 70%. The good storage performance and the stability of the LFP-700 film could be mainly attributed to feature properties of the $Li_3Fe_2(PO_4)_3$ thin film. Compared to LFP-700 sample, the sharp capacity dropping of LFP-400, LFP-500 and LFP-600 in the first few cycles can be imputed to the cracks that are responsible for the poor mechanical properties. For more details, the areal capacity values and the capacity retention at the 50th and 100th cycles are summarized in Table 1.

As a further examination, we also studied the rate capability of the thin films annealed at 500 °C and 700 °C because they showed the most interesting electrochemical properties (Fig. 8b). LFP-500 delivers stable capacity values of 35 $\mu Ah\ cm^{-2}\ \mu m^{-1}$ at C/10 rate, 25 $\mu Ah\ cm^{-2}\ \mu m^{-1}$ at C/5 rate, and 13 $\mu Ah\ cm^{-2}\ \mu m^{-1}$ at 1C rate. Although the initial C/10 and C/5 discharge capacity are superior compared to LFP-700 film, the LFP-500 shows relatively larger degradation in capacity with further increasing discharge current. Indeed, significant capacity losses of 28% and 48% are observed for subsequent tests at C/5 and 1C rate, respectively. The LFP-700 film cathode delivers capacity values of 25 $\mu Ah\ cm^{-2}\ \mu m^{-1}$ at C/10 rate, 22 $\mu Ah\ cm^{-2}\ \mu m^{-1}$ at C/5 rate, and 19 $\mu Ah\ cm^{-2}\ \mu m^{-1}$ at 1C rate. The capacity slightly decreased of only 11% from C/10 to C/5 rate and decreased of about 15.5% from C/5 to 1C rate. More remarkably, the discharge capacity values of about 22 $\mu Ah\ cm^{-2}\ \mu m^{-1}$ and 25 $\mu Ah\ cm^{-2}\ \mu m^{-1}$ at C/5 and C/10 show that the full capacity is completely recovered even after fast cycling tests. Therefore, it is found that the highest annealing temperature treatment (700 °C) is able to strongly improve the electrochemical stability of LFP films electrodes, especially in the rapid charge-discharge regimes. After few initial cycles, LFP-700 film reveals high reversibility and prominent cycling stability. The better performance of LFP-700 film is also attributed to the presence of the LTP phase as a good ionic conductor[56].

To sum up, the amorphous and partially crystalline LFP phases may not be stable during Li-ion intercalation/de-intercalation, yielding in a fast capacity fading[22]. Thus, through this study, we highlight the important role of the post annealing treatment mainly for the intercalation cathodes. This treatment is responsible for the film texturation, thus it could help minimizing ionic limitation by enhancing the contact area between electrolyte and the film surface contact, as well as could enhance the electrochemical activity[54,57–59].

Conclusion

In summary, we have successfully prepared porous thin film cathodes by RF sputtering technique and subsequent annealing treatment in air atmosphere. The electrochemical performance of the thin films depends strongly on the annealing conditions. Different morphological and structural properties were obtained by varying the temperature treatment, leading to a significant influence on the cell performances. We report that annealing at 500 °C is required to obtain porous olivine type-$LiFePO_4$ film even if the electrochemical tests revealed a drop of capacities after the 80th cycle. Complete transformation from porous olivine type-$LiFePO_4$ to porous NASICON-type $Li_3Fe_2(PO_4)_3$ occurring at 700 °C led to a remarkable stability of the electrode with good electrochemical performance even at fast kinetics.

Methods

Preparation of LFP thin films. Thin films were deposited on Ti foil substrate by radio frequency sputtering in a Plassys MP 300 apparatus at room temperature. In the present work, radio-frequency (RF) sputtering is utilized to deposit LFP layers from a commercial target. The target was $LiFePO_4$ (LFP) purchased from Neyco, purity 99.9%. Prior to their insertion in the deposition chamber, Ti foils were cleaned by ultrasonication in acetone, 2-propanol, and methanol for 10 minutes each. Pre-sputtering of the targets before deposition was employed to remove the native oxide layer. Before deposition, vacuum was applied into the sputtering chamber until the pressure was around 3×10^{-6} mbarr. Sputtering was performed in a pure argon atmosphere. The argon pressure was set to 7 mTorr and the applied RF sputtering power was fixed to 75 W (3 W cm^{-2}). Deposition time was adjusted for 12 hours. The post-annealing treatment was carried out at various temperatures (400 °C, 500 °C, 600 °C, and 700 °C) for one hour with a heating rate of 2 °C min^{-1} (Furnace: NABERTHERM Controller B 180). The as-deposited thin film was labelled as LFP-0 and post-annealed thin films at 400 °C, 500 °C, 600 °C and 700 °C were labelled as LFP-400, LFP-500, LFP-600, and LFP-700, respectively.

Materials characterization. The crystalline structure of the initial $LiFePO_4$ target and as-deposited film were analyzed by X-ray diffraction in a D5000 BRUKER-SIEMENS diffractometer with Cu-Kα radiation (wavelength = 1.5406 Å) over 2θ range of 10–70°. The accelerating voltage and current were 40 kV and 30 mA, respectively and a scan speed of 0.04° per second was utilized. The *in-situ* X-ray diffraction measurement was also performed on an X'Pert diffractometer with Cu-Kα radiation. As-deposited LFP film was mounted on an adapted furnace and annealed from 400 °C to 700 °C with an interval of 20 °C. The data were collected every 300 s with scan-step size 0.04°. The diffractogramms were analyzed using JCPDS-ICDD (Joint Committee on Powder Diffraction Standards-International Center for Diffraction Data). Morphological properties of the thin films were characterized by Scanning Electron Microscopy (SEM) using a field-emission scanning electron microscope (Ultra-55 Carl Zeiss).

Electrochemical measurements. All cells were assembled in an argon-filled glove box (MBraun, Germany) with H_2O and O_2 contents were less than 0.5 ppm. The electrochemical properties of the LFP thin films (LFP-0, LFP-400, LFP-500, LFP-600, and LFP-700) were evaluated by cyclic voltammetry (CV) and chronopotentiometry using a VMP3 potentiostat (Bio Logic, France). For the electrochemical tests, two-electrode Swagelok cells were assembled using the LFP thin films as the working electrode while metallic lithium foils served as both the counter and the reference electrodes. It is important to specify that the electrodes were not mixed with any additive and binder. The working and counter electrodes were separated by a Whatman glass microfiber soaked in the liquid organic electrolyte composed of 1 mol L^{-1} of $LiPF_6$ in ethylene carbonate (EC) – diethyl carbonate (DEC) (1:1 in w/w). The area of the LFP films was 0.49 cm^2 and the average thickness of the film was ca. 1.6 µm, measured from cross section SEM images. The CV measurement was performed in the potential range between 2 and 4 V at a scan rate of 0.1 mV s^{-1} and galvanostatic cycling with potential limitation (GCPL) was performed in the potential range in the same potential window at multiple C-rates (C/10, C/5, C/2 and 1C). The charge or discharge rate denoted as C/*n* means that the battery is fully charged or discharged up to its total storage capacity in *n* hours, whilst C-rate of the LFP films were calculated by estimating the weight of active material in the thin film from the film thickness and the density of 3.6 g cm^{-3}.

References

1. Ortiz, G. F. *et al.* Alternative Li-Ion Battery Electrode Based on Self-Organized Titania Nanotubes. *Chem. Mater.* **21**, 63–67 (2009).
2. Fraoucene, H. *et al.* Optical and Electrochemical Properties of Self-Organized TiO2 Nanotube Arrays From Anodized Ti–6Al–4V Alloy. *Front. Chem.* **7** (2019).
3. Laïk, B. *et al.* Silicon nanowires as negative electrode for lithium-ion microbatteries. *Electrochimica Acta* **53**, 5528–5532 (2008).
4. Perre, E. *et al.* Electrodeposited Cu_2Sb as anode material for 3-dimensional Li-ion microbatteries. *Journal of Materials Research* **25**, 1485–1491 (2010).
5. Oltean, G., Asfaw, H. D., Nyholm, L. & Edström, K. A Li-Ion Microbattery with 3D Electrodes of Different Geometries. *ECS Electrochem. Lett.* **3**, A54–A57 (2014).
6. Sharifi, T. *et al.* Hierarchical self-assembled structures based on nitrogen-doped carbon nanotubes as advanced negative electrodes for Li-ion batteries and 3D microbatteries. *Journal of Power Sources* **279**, 581–592 (2015).
7. Sugiawati, V. A., Vacandio, F., Ein-Eli, Y. & Djenizian, T. Electrodeposition of polymer electrolyte into carbon nanotube tissues for high performance flexible Li-ion microbatteries. *APL Materials* **7**, 031506 (2019).
8. Reddy, M. V., Pecquenard, B., Vinatier, P. & Levasseur, A. Effect of Substrate Temperature on Morphology and Electrochemical Performance of Radio Frequency Magnetron Sputtered Lithium Nickel Vanadate Films Used as Negative Electrodes for Lithium Microbatteries. *J. Phys. Chem. B* **110**, 4301–4306 (2006).
9. Padhi, A. K., Nanjundaswamy, K. S. & Goodenough, J. B. Phospho olivines as Positive–Electrode Materials for Rechargeable Lithium Batteries. *J. Electrochem. Soc.* **144**, 1188–1194 (1997).
10. Ni, Q., Bai, Y., Wu, F. & Wu, C. Polyanion–Type Electrode Materials for Sodium–Ion Batteries. *Adv Sci (Weinh)* **4** (2017).
11. Li, Q., Chou, S.-L., Wang, J.-Z., Shi, D. & Liu, H.-K. Highly oriented $LiFePO_4$ thin film electrodes via chemical solution deposition. *Solid State Ionics* **268**, 117–124 (2014).
12. Sugiawati, V. A., Vacandio, F., Eyraud, M., Knauth, P. & Djenizian, T. Porous NASICON-Type $Li_3Fe_2(PO_4)_3$ Thin Film Deposited by RF Sputtering as Cathode Material for Li-Ion Microbatteries. *Nanoscale Res Lett* **11** (2016).
13. Fujimoto, D., Kuwata, N., Matsuda, Y., Kawamura, J. & Kang, F. Fabrication of solid-state thin-film batteries using $LiMnPO_4$ thin films deposited by pulsed laser deposition. *Thin Solid Films* **579**, 81–88 (2015).
14. Sugiawati, V. A., Vacandio, F., Knauth, P. & Djenizian, T. Sputter-Deposited Amorphous $LiCuPO_4$ Thin Film as Cathode Material for Li-ion Microbatteries. *ChemistrySelect* **3**, 405–409 (2018).
15. Zhu, X.-J. *et al.* Preparation and Characteristics of $LiFePO_4$ Thin Film by Radio Frequency Magnetron Sputtering for Lithium Microbatteries. *J. Phys. Chem. C* **113**, 14518–14522 (2009).
16. Bouwman, P. J., Boukamp, B. A., Bouwmeester, H. J. M. & Notten, P. H. L. Influence of Diffusion Plane Orientation on Electrochemical Properties of Thin Film $LiCoO_2$ Electrodes. *J. Electrochem. Soc.* **149**, A699–A709 (2002).
17. Iriyama, Y. *et al.* Preparation of $LiFePO_4$ Thin Films by Pulsed Laser Deposition and Their Electrochemical Properties. *Electrochem. Solid-State Lett.* **7**, A340–A342 (2004).
18. Yada, C. *et al.* Electrochemical properties of $LiFePO_4$ thin films prepared by pulsed laser deposition. *Journal of Power Sources* **146**, 559–564 (2005).
19. Lu, Z. G., Cheng, H., Lo, M. F. & Chung, C. Y. Pulsed Laser Deposition and Electrochemical Characterization of $LiFePO_4$–Ag Composite Thin Films. *Advanced Functional Materials* **17**, 3885–3896 (2007).
20. Sun, J., Tang, K., Yu, X., Li, H. & Huang, X. Needle-like $LiFePO_4$ thin films prepared by an off-axis pulsed laser deposition technique. *Thin Solid Films* **517**, 2618–2622 (2009).
21. Palomares, V. *et al.* $LiFePO_4$ thin films grown by pulsed laser deposition: Effect of the substrate on the film structure and morphology. *Applied Surface Science* **256**, 2563–2568 (2010).
22. Deng, J. *et al.* Electrochemical performance of $LiNi_{1/3}Co_{1/3}Mn_{1/3}O_2$ thin film electrodes prepared by pulsed laser deposition. *Journal of Power Sources* **217**, 491–497 (2012).
23. Xie, J. *et al.* Li-ion diffusion kinetics in $LiFePO_4$ thin film prepared by radio frequency magnetron sputtering. *Electrochimica Acta* **54**, 4631–4637 (2009).
24. Chiu, K.-F. Optimization of Synthesis Process for Carbon-Mixed $LiFePO_4$ Composite Thin-Film Cathodes Deposited by Bias Sputtering. *J. Electrochem. Soc.* **154**, A129–A133 (2007).
25. Rho, Y. H. *et al.* Preparation of $Li_4Ti_5O_{12}$ and $LiCoO_2$ thin film electrodes from precursors obtained by sol–gel method. *Solid State Ionics* **151**, 151–157 (2002).

26. Kim, M.-K. *et al*. Fabrication of $LiCoO_2$ thin films by sol–gel method and characterisation as positive electrodes for Li/$LiCoO_2$ cells. *Journal of Power Sources* **99**, 34–40 (2001).
27. Park, Y. J., Kim, J. G., Kim, M. K., Chung, H. T. & Kim, H. G. Preparation of $LiMn_2O_4$ thin films by a sol–gel method. *Solid State Ionics* **130**, 203–214 (2000).
28. Bates, J. B. *et al*. Preferred Orientation of Polycrystalline $LiCoO_2$ Films. *J. Electrochem. Soc.* **147**, 59–70 (2000).
29. Lee, H., Kim, S., Kim, K.-B. & Choi, J.-W. Scalable fabrication of flexible thin-film batteries for smart lens applications. *Nano Energy* **53**, 225–231 (2018).
30. Oukassi, S. *et al*. Transparent Thin Film Solid-State Lithium Ion Batteries. *ACS Applied Materials & Interfaces*, https://doi.org/10.1021/acsami.8b16364 (2018).
31. Cabana, J., Shirakawa, J., Nakayama, M., Wakihara, M. & Grey, C. P. Effect of ball-milling and lithium insertion on the lithium mobility and structure of $Li_3Fe_2(PO_4)_3$. *J. Mater. Chem.* **21**, 10012–10020 (2011).
32. Karami, H. & Taala, F. Synthesis, characterization and application of $Li_3Fe_2(PO_4)_3$ nanoparticles as cathode of lithium-ion rechargeable batteries. *Journal of Power Sources* **196**, 6400–6411 (2011).
33. Yang, Y. *et al*. Effect of VO43– substitution for PO43– on electrochemical properties of the $Li_3Fe_2(PO_4)_3$ cathode materials. *Electrochimica Acta* **219**, 547–552 (2016).
34. Salah, A. A. *et al*. Local structure and redox energies of lithium phosphates with olivine- and Nasicon-like structures. *Journal of Power Sources* **140**, 370–375 (2005).
35. Sun, J.-K. *et al*. Characterization of Nasicon-type $Li_3Fe_{2-2x}Ti_xMn_x(PO_4)_{3/C}$ cathode materials. *Journal of Alloys and Compounds* **469**, 327–331 (2009).
36. Yang, S., Zavalij, P. Y. & Stanley Whittingham, M. Hydrothermal synthesis of lithium iron phosphate cathodes. *Electrochemistry Communications* **3**, 505–508 (2001).
37. Ivanov-Schitz, A. K., Nistuk, A. V. & Chaban, N. G. $Li_3Fe_2(PO_4)_3$ solid electrolyte prepared by ultrasonic spray pyrolysis. *Solid State Ionics* **139**, 153–157 (2001).
38. Tintignac, S., Baddour-Hadjean, R., Pereira-Ramos, J.-P. & Salot, R. High performance sputtered $LiCoO_2$ thin films obtained at a moderate annealing treatment combined to a bias effect. *Electrochimica Acta* **60**, 121–129 (2012).
39. Chiu, K.-F. & Chen, P. Y. Structural evolution and electrochemical performance of $LiFePO_{4/C}$ thin films deposited by ionized magnetron sputtering. *Surface and Coatings Technology* **203**, 872–875 (2008).
40. Sauvage, F., Baudrin, E., Laffont, L. & Tarascon, J.-M. Origin of electrochemical reactivity enhancement of post-annealed $LiFePO_4$ thin films: Preparation of heterosite-type FePO4. *Solid State Ionics* **178**, 145–152 (2007).
41. Hamelet, S. *et al*. The effects of moderate thermal treatments under air on $LiFePO_4$–based nano powders. *J. Mater. Chem.* **19**, 3979–3991 (2009).
42. Delacourt, C., Poizot, P., Tarascon, J.-M. & Masquelier, C. The existence of a temperature-driven solid solution in Li_xFePO_4 for $0 \leq x \leq 1$. *Nature Materials* **4**, 254–260 (2005).
43. Bünting, A. *et al*. Influence of titanium nitride interlayer on the morphology, structure and electrochemical performance of magnetron-sputtered lithium iron phosphate thin films. *Journal of Power Sources* **281**, 326–333 (2015).
44. Yu, S. *et al*. $LiTi_2(PO_4)_{3/C}$ Anode Material with a Spindle–Like Morphology for Batteries with High Rate Capability and Improved Cycle Life. *ChemElectroChem* **3**, 1157–1169 (2016).
45. Guan, X., Li, G., Li, C. & Ren, R. Synthesis of porous nano/micro structured $LiFePO_{4/C}$ cathode materials for lithium-ion batteries by spray-drying method. *Transactions of Nonferrous Metals Society of China* **27**, 141–147 (2017).
46. Wu, J., Cai, W. & Shang, G. Electrochemical Behavior of $LiFePO_4$ Thin Film Prepared by RF Magnetron Sputtering in Li_2SO_4 Aqueous Electrolyte. *Int. J. Nanosci.* **14**, 1460027 (2014).
47. Wang, J. *et al*. Nature of $LiFePO_4$ aging process: Roles of impurity phases. *Journal of Power Sources* **238**, 454–463 (2013).
48. Asl, H. Y. & Choudhury, A. Phosphorous acid route synthesis of iron tavorite phases, $LiFePO_4(OH)_xF_{1-x}$ $[0 \leq x \leq 1]$ and comparative study of their electrochemical activities. *RSC Adv.* **4**, 37691–37700 (2014).
49. Marx, N. *et al*. The structure of tavorite $LiFePO_4(OH)$ from diffraction and GGA + U studies and its preliminary electrochemical characterization. *Dalton Trans.* **39**, 5108–5116 (2010).
50. Masquelier, C., Padhi, A. K., Nanjundaswamy, K. S. & Goodenough, J. B. New Cathode Materials for Rechargeable Lithium Batteries: The 3-D Framework Structures $Li_3Fe_2(XO_4)_3$ (X = P, As). *Journal of Solid State Chemistry* **135**, 228–234 (1998).
51. Padhi, A. K., Nanjundaswamy, K. S., Masquelier, C. & Goodenough, J. B. Mapping of Transition Metal Redox Energies in Phosphates with NASICON Structure by Lithium Intercalation. *J. Electrochem. Soc.* **144**, 2581–2586 (1997).
52. Padhi, A. K., Nanjundaswamy, K. S., Masquelier, C., Okada, S. & Goodenough, J. B. Effect of Structure on the Fe^{3+}/Fe^{2+} Redox Couple in Iron Phosphates. *J. Electrochem. Soc.* **144**, 1609–1613 (1997).
53. Legrand, C. *et al*. Structural and textural characterization of $LiFePO_4$ thin films prepared by pulsed laser deposition on Si substrates. *Thin Solid Films* **518**, 5447–5451 (2010).
54. Sauvage, F., Baudrin, E., Gengembre, L. & Tarascon, J.-M. Effect of texture on the electrochemical properties of $LiFePO_4$ thin films. *Solid State Ionics* **176**, 1869–1876 (2005).
55. Zhou, Y., Wang, J., Hu, Y., O'Hayre, R. & Shao, Z. A porous $LiFePO_4$ and carbon nanotube composite. *Chem. Commun.* **46**, 7151–7153 (2010).
56. Zając, W., Tarach, M. & Trenczek-Zając, A. Towards control over redox behaviour and ionic conductivity in $LiTi_2(PO_4)_3$ fast lithium-ion conductor. *Acta Materialia* **140**, 417–423 (2017).
57. Nanjundaswamy, K. S. *et al*. Synthesis, redox potential evaluation and electrochemical characteristics of NASICON-related-3D framework compounds. *Solid State Ionics* **92**, 1–10 (1996).
58. Andersson, A. S. *et al*. Lithium insertion into rhombohedral $Li_3Fe_2(PO_4)_3$. *Solid State Ionics* **140**, 63–70 (2001).
59. Morcrette, M., Wurm, C. & Masquelier, C. On the way to the optimization of $Li_3Fe_2(PO_4)_3$ positive electrode materials. *Solid State Sciences* **4**, 239–246 (2002).

Acknowledgements

This work is financially supported by the Région SUD.

Author Contributions

T.D. and F.V. supervised the work. V.A.S. conducted the experiments. C.P., A.G., and A.P.K. contributed to the discussion. All authors have reviewed the manuscript.

Additional Information

Competing Interests: The authors declare no competing interests.

Publisher's note: Springer Nature remains neutral with regard to jurisdictional claims in published maps and institutional affiliations.